APEM journal
**Advances in Production Engineering & Management**
Volume 18 | Number 3 | September 2023 | pp 371–380
https://doi.org/10.14743/apem2023.3.479
**ISSN 1854-6250**
Journal home: apem-journal.org
Original scientific paper

# Optimization of machining performance in deep hole boring: A study on cutting tool vibration and dynamic vibration absorber design

**Li, L.**[a,*], **Yang, D.L.**[a], **Cui, Y.M.**[a]

[a]School of Mechatronic Engineering, Jiangsu Normal University, Xuzhou, P.R. China

**ABSTRACT**

In the realm of precision engineering, particularly in deep hole boring processes, tool vibration emerges as a critical determinant of machining performance. This investigation elucidates the genesis of self-excited vibrations within deep hole boring operations and delineates the underlying mechanisms of cutting tool vibration. A focal point of this study is the optimal alignment of the boring bar to mitigate vibrational impacts, thereby enhancing surface finish quality and extending tool longevity. Central to this analysis is the employment of a Dynamic Vibration Absorber (DVA) aimed at attenuating cutting tool vibration. The deployment of DVA necessitates precise identification of modal parameters, namely the equivalent stiffness ($K$) and mass ($M$) of the cutting tool. This research juxtaposes various scholarly methodologies to amalgamate theoretical calculations with simulation approaches, thereby acquiring accurate modal parameters. Utilizing Matlab software, the vibration amplitude of the boring bar under varying spring stiffness scenarios was examined. Results indicate a direct correlation between increased stiffness and reduced amplitude, particularly when the frequency ratio $g$ ranges between 0.5 and 1.1. Consequently, a stiffer DVA configuration is posited as more effective in vibration reduction. Furthermore, the study conducted frequency sweep experiments on a damping boring bar, utilizing a vibration excitation platform. These experiments revealed the existence of an optimal stiffness value for the DVA, thereby underscoring the significance of stiffness matching in vibration mitigation strategies.

**ARTICLE INFO**

*Keywords:*
Deep hole boring;
Boring bar;
Machining performance;
Vibration;
Dynamic vibration absorber;
Stiffness matching;
Matlab

**Corresponding author:*
6020190159@jsnu.edu.cn
(Li, L.)

*Article history:*
Received 20 May 2023
Revised 12 November 2023
Accepted 17 November 2023



## 1. Introduction

In the domain of machining operations, tool vibration has been identified as a pivotal factor impacting surface quality, material removal rates, and tool wear longevity [1-7]. Predominantly, self-excited vibrations manifest as the primary vibration type within machining contexts [8]. Chatter, a frequent occurrence, is typically initiated when the external excitation frequency aligns closely with the natural frequency of cutting tools. Intriguingly, a discrepancy between the excitation and natural frequencies, as depicted in Fig. 1, does not preclude chatter; it may arise owing to the phase differential between surface positions $x(t)$ and $x(t-T)$ at distinct temporal intervals. Variability in cutting thickness, $h$, during machining induces tool movement instability. Consequently, the excitation force encompasses a spectrum of frequencies, modulating in response to alterations in cutting parameters and workpiece materials [9, 10].

The underlying cause of vibration issues is often traced to inadequate damping within the structural framework. The most straightforward remedial approach involves augmenting exter-

nal damping to the mechanical structure. Yet, this strategy encounters limitations due to structural and spatial constraints, rendering its application scope somewhat limited. Over the past century, the development of DVA has emerged as a viable solution for vibration reduction. Its ease of implementation and simplistic design have garnered acclaim [11]. Several scholars [12, 13] have undertaken simulation analyses to explore the impact of controlled vibration on surface roughness.

Fig. 2 illustrates the DVA, comprising a mass *m*, spring *k*, and damping *c*, a concept first introduced by Ormondroyd and Den Hartog in 1928 [14]. The Vibration Controlled System (VCS), consisting of mass *M* and spring *K*, integrates the DVA as an auxiliary kinetic system, thereby facilitating vibration energy absorption.

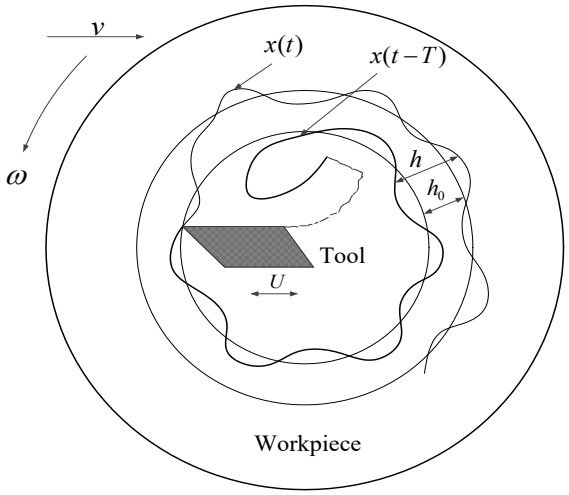


**Fig. 1** Mechanism of regeneration

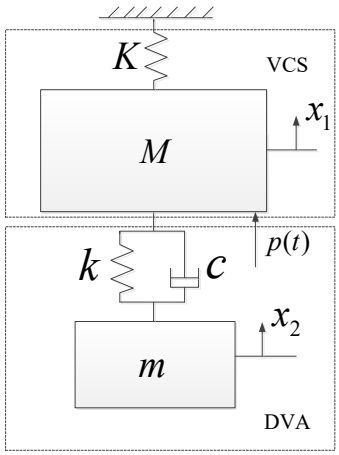


**Fig. 2** Dynamic model of DVA

Prior to the design of DVA, it is imperative to accurately ascertain the equivalent stiffness ($K$) and mass ($M$) of the cutting tool. Subsequently, the parameters of DVA, i.e., mass ($m$), spring constant ($k$), and damping coefficient ($c$), are determined through the application of dynamic mathematical methods.

The kinetic equation of the dynamic model, as illustrated in Fig. 2, is presented as follows [15]:

$$\begin{cases} M\ddot{x}_1 + c\dot{x}_1 + (k+K)x_1 - c\dot{x}_2 - kx_2 = p(t) \\ m\ddot{x}_2 + c\dot{x}_2 + kx_2 - c\dot{x}_1 - kx_2 = 0 \end{cases} \tag{1}$$

where $p(t) = p_0 \sin \omega t$ is used to simulate external excitation signals.

Through a complex derivation process [16-19], the vibration amplitude of the VCS is derived:

$$A(g) = \sqrt{\frac{(2\zeta g)^2 + (g^2 - f^2)}{(2\zeta g)^2(g^2 - 1 + \mu g^2)^2 + [\mu f^2 g^2 - (g^2 - 1)(g^2 - f^2)]^2}} \tag{2}$$

where $\zeta$ is the damping ratio given by $\zeta = c/(2\sqrt{mk})$, $\mu$ is the mass ratio given by $\mu = m/M$, $g$ is the frequency ratio given by $g = \omega/\omega_n$, here $\omega_n$ is the natural frequency of the main mass $M$ given by $\omega_n = \sqrt{K/M}$, $f$ is the natural frequency ratio given by $f = \omega_a/\omega_n$, here $\omega_a$ is the natural frequency of the DVA given by $\omega_a = \sqrt{k/m}$.

The objective is to minimize the vibration amplitude of the VCS. Upon determining the VCS parameters, the next step involves selecting optimal parameters for the DVA to achieve exemplary vibration reduction. Generally, to minimize the DVA's volume, the mass $m$ should be set as large as possible. Given that the cutting tool body is typically composed of metal materials, the damping coefficient $c$ is relatively small, predominantly affecting the peak height of the VCS's vibration amplitude, while exerting minimal influence on the resonance frequency. Consequently, the primary parameter of concern is the spring constant $k$.

Achieving optimal vibration reduction hinges on two critical factors: accurately determining the modal parameters of the cutting tool and identifying the optimal stiffness $k$. The modeling of the boring bar has been a subject of extensive research by several eminent scholars [20-23]. Tewani *et al*. [24] conceptualize the boring bar as an equivalent constant-section beam. Seto [25] has proposed equivalent methods for calculating the boring bar's parameters.

This study undertakes the theoretical modeling and analysis of the boring bar using three distinct methods. Subsequently, the impact of the absorber's stiffness on the amplitude of the boring bar is examined using Matlab. Finally, a frequency sweep experiment of the damping boring bar is conducted on a vibration excitation platform, yielding some noteworthy results.

## 2. Theoretical analysis

As depicted in Fig. 3, the boring bar functions akin to a cantilever beam during the cutting process. During this operation, the cutting head is subjected to a wide-band signal, potentially inducing multiple vibration modes within the boring bar.

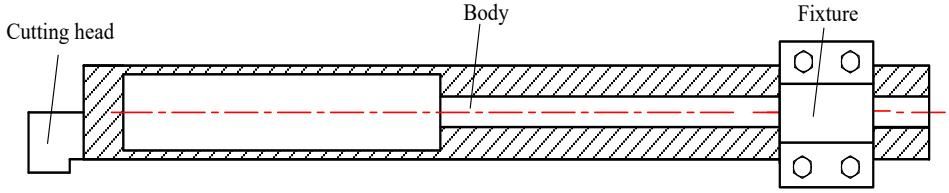


**Fig. 3** Boring bar

Utilizing Abaqus software facilitates the determination of the boring bar's natural frequencies. Fig. 4 illustrates these frequencies as 350.58 Hz, 350.98 Hz, 1837.5 Hz, and 1840.1 Hz, respectively. However, the energy of high-frequency signals is comparatively weak, rarely manifesting in typical operations. Consequently, the primary focus is typically on the first-order frequency. It is evident that the lower natural frequencies are associated with bending vibrations of the boring bar.

Given the significance of the first-order bending vibration in the boring bar, the system is simplified for computational efficiency by modeling it as a one-degree-of-freedom system. This model, as illustrated in Fig. 5, is comprised of a spring and a mass, effectively capturing the essential dynamics of the boring bar's behavior.

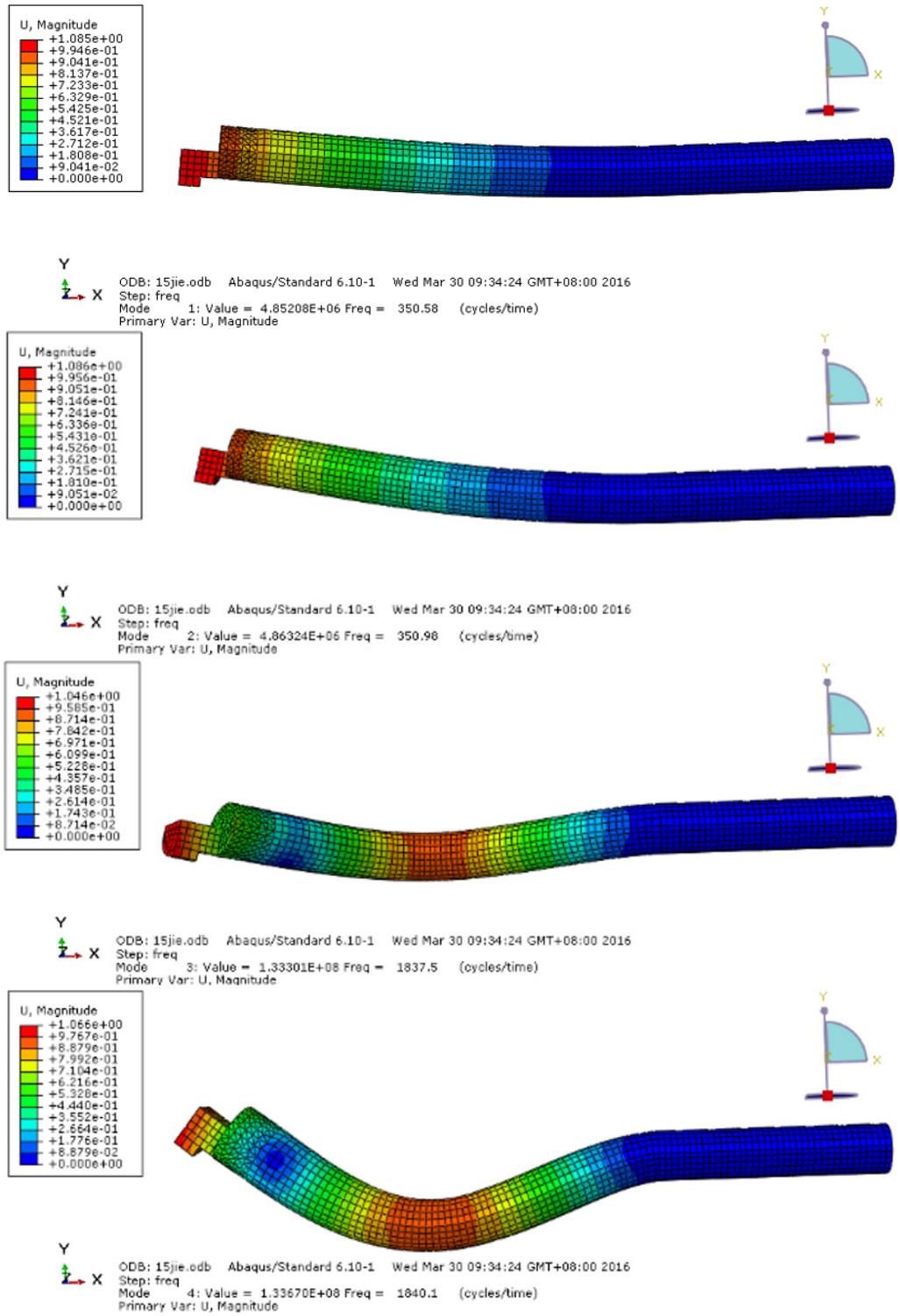


**Fig. 4** Natural frequency of the boring bar

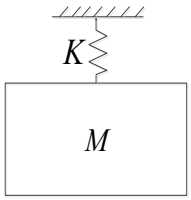


**Fig. 5** Modeling of the boring bar

The equations for determining the equivalent stiffness and mass of the boring bar are as follows:

$$K = \frac{3EI}{L^3} \tag{3}$$

where $L$ represents the length of the boring bar, $E$ is the modulus of elasticity, and $I$ denotes the moment of inertia.

The first-order natural frequency of a clamped beam is calculated using the equation:

$$\omega_n = 3.52\sqrt{\frac{EI}{\rho L^4}} \tag{4}$$

where $\rho$ is the mass per unit length of the boring bar.

Then, we get the equivalent mass:

$$M = \frac{K}{{\omega_n}^2} \tag{5}$$

Apart from the aforementioned computational methods, the equivalent mass can also be estimated using an empirical formula:

$$M = m_o + 0.243m_b \tag{6}$$

where, $m_o$ is the head mass of the boring bar, $m_b$ is the body mass of the hollow boring bar.

Both these calculation approaches treat the boring bar as a beam with a constant cross-section. Nonetheless, for the purposes of integrating the DVA, the boring bar often features a variable cross-section. To acquire more precise values for equivalent stiffness and mass, a method that accounts for cavities in the boring bar is proposed. As illustrated in Fig. 6, a force applied at the DVA's geometric center causes a minor displacement, $d_E$, which can be quantified using the piece-wise superposition theory. Consequently, the equivalent stiffness is deduced as per Eq. 7:

$$K = \frac{F}{d_E} = \frac{F}{d_{E0} + d_C + \frac{1}{2}\theta_C l_2} = \frac{1}{\frac{4{l_1}^3 + 6{l_1}^2 l_2 + 3l_1{l_2}^2}{12EI_1} + \frac{F{l_2}^3}{24EI_2}} \tag{7}$$

where $I_1$ and $I_2$ are the inertia moments of AC and CD separately.

This is illustrated in Fig. 7, where the gravity acting on the boring bar induces a displacement, *s*, at point *E*. This displacement is analogous to the effect of applying a concentrated mass, *M*.

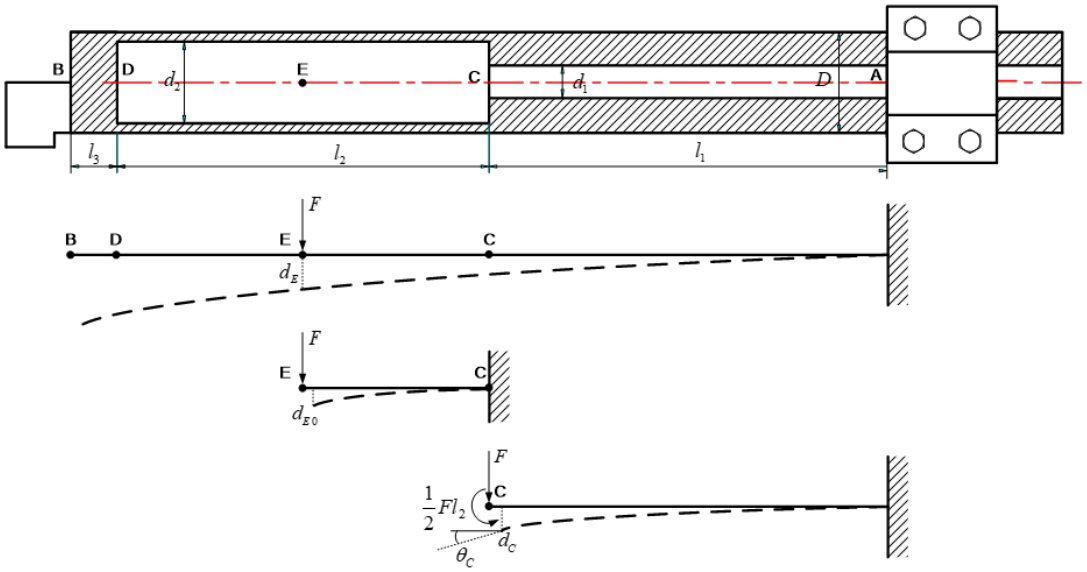


**Fig. 6** Modeling of equivalent stiffness

Consequently, the equivalent mass is determined as follows:

$$M = \frac{Ks}{g} \tag{8}$$

where $s$ is obtained:

$$\begin{aligned} s = s_1 + s_2 + s_3 = {} & \frac{q_1 l_1^4}{8EI_1} + \frac{q_1 l_1^3 l_2}{12EI_1} + \frac{q_2 l_1^2 l_2^2}{3EI_1} + \frac{q_2 l_1^2 l_2^2}{2EI_1} \\ & + \frac{q_2 l_1 l_2^3}{4EI_1} + \frac{17 q_2 l_2^4}{384EI_2} + \frac{q_3 l_1^3 l_3}{3EI_1} + \frac{3 q_3 l_1^2 l_2 l_3}{4EI_1} + \frac{q_3 l_1^2 l_3^2}{4EI_1} + \frac{q_3 l_1 l_2^2 l_3}{2EI_1} \\ & + \frac{q_3 l_1 l_2 l_3^2}{4EI_1} + \frac{5 q_3 l_2^3 l_3}{48EI_2} + \frac{q_3 l_2^2 l_3^2}{16EI_2} \end{aligned} \tag{9}$$

where $s_1$, $s_2$, $s_3$ denote the displacements of the boring bar at point E, attributable to the gravitational forces acting on different segments, as depicted in Fig. 8.

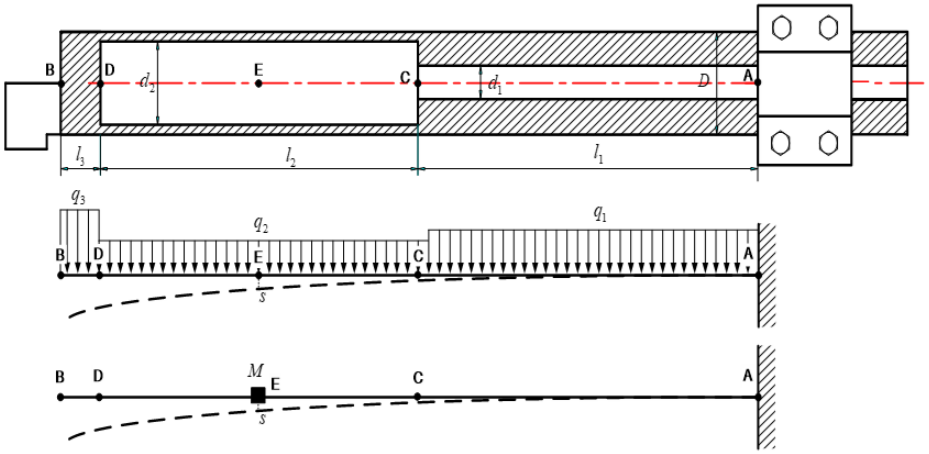


**Fig. 7** Modeling of equivalent mass

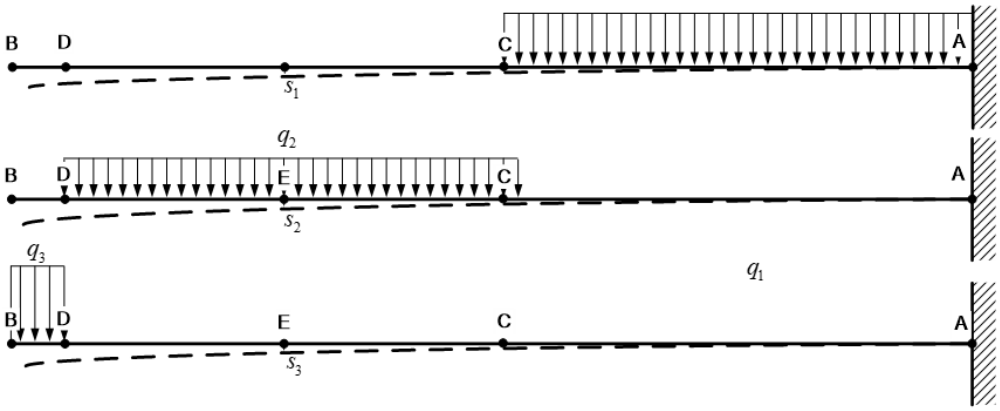


**Fig. 8** Displacements under different segment's gravity

Utilizing the aforementioned three methods of calculation, results for the equivalent stiffness and mass of the boring bar have been obtained, as summarized in Table 1. In comparison with the simulation result, which indicated a natural frequency of 351 Hz, the error values have also been calculated.

**Table 1** Results by using different calculation methods

| Method | Equivalent stiffness (N/mm) | Equivalent mass (kg) | Frequency (Hz) | Error value (Hz) |
|---|---|---|---|---|
| 1 | 2428 | 2.301 | 163.5 | -186.5 |
| 2 | 2428 | 0.671 | 302.7 | -48.3 |
| 3 | 2492 | 0.447 | 375.8 | +24.8 |

It is evident that a degree of error is inherent in each calculation method used. A notable observation is the variation in equivalent mass values derived from different methods, which significantly contributes to the overall error margin. To mitigate this issue, a combined approach integrating theoretical calculations with simulation methods is employed to identify the vibration modal parameters of the boring bar more accurately. Initially, Eq. 7 is utilized to ascertain the equivalent stiffness. Subsequently, the natural frequency is determined using Abaqus, as illustrated in Fig. 4. Finally, the equivalent mass is calculated employing the equation:

$$M = \frac{K}{4\pi^2 f^2} \tag{10}$$

Fig. 9 depicts the structure of the DVA, which comprises two springs and an inner core. This assembly is filled with silicone oil. Notably, the stiffness of the DVA can be adjusted by modifying the end cap, allowing for fine-tuning of the absorber's properties to suit specific vibration control requirements.

In this study, the specific parameters under consideration are: $K = 2492$ N/mm, $M = 0.512$ kg, $m = 0.9162$ kg, $c = 237$ kg/s. Utilizing Matlab, as illustrated in Fig. 10, the vibration amplitude of the VCS is calculated across a range of spring stiffness values.

An analysis of the resultant curve reveals two distinct peaks. It is observed that as the stiffness increases, the amplitude of the first peak also rises, which is contrary to the desired outcome. However, it is important to note that the machine's excitation frequency component typically exceeds 200 Hz. This implies that the damping boring bar becomes effective when the parameter $g$ is greater than 0.57. As depicted in Fig. 10, within the range of 0.5 to 1.1 for the parameter $g$, an increase in stiffness correlates with a reduction in amplitude. Therefore, to achieve more effective vibration reduction, a preference for higher stiffness is suggested.

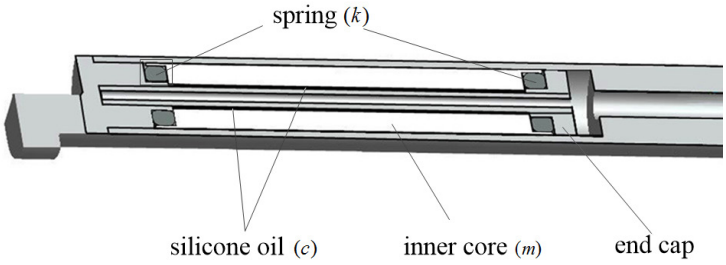


**Fig. 9** Structure of the DVA

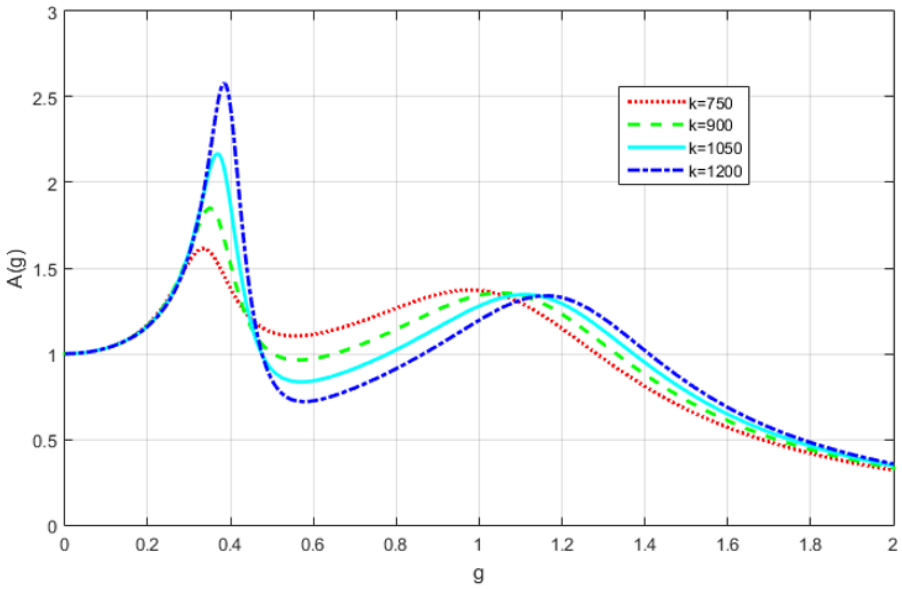


**Fig. 10** Vibration amplitude of the VCS under different spring stiffness

## 3. Experimental work

To corroborate the analytical results, a frequency sweep experiment was conducted on a vibration excitation platform, as depicted in Fig. 11. This platform can generate a sine signal with a frequency range spanning from 20 Hz to 1200 Hz. The input control channel, responsible for maintaining the amplitude of the input signal at 1g, is strategically positioned at the tail end of the boring bar.

The experiment was conducted under four distinct conditions, paralleling the simulations previously described.

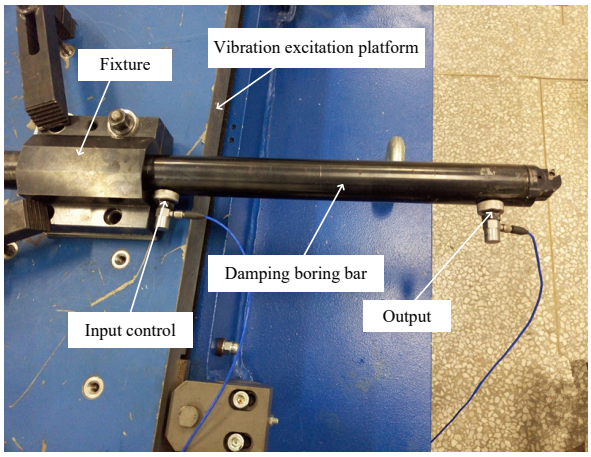


**Fig. 11** Frequency sweep experiment

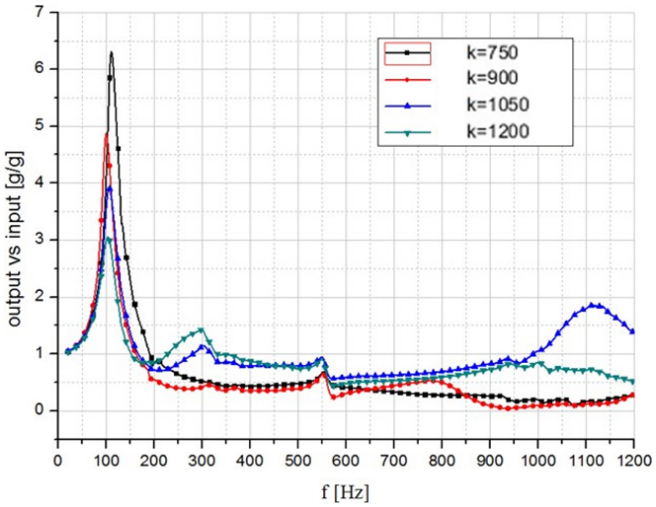


**Fig. 12** Harmonic response under four different conditions

Fig. 12 presents the results of the experiment, and when compared with Fig. 10, the trends in both figures are observed to be consistent. The following key observations can be made: (1) While the spring stiffness does affect the first-order natural frequency, this impact is relatively subtle, with recorded frequencies at 110 Hz, 100 Hz, 105 Hz, and 103 Hz, respectively; (2) An increase in stiffness leads to a higher peak amplitude of the first-order natural frequency; (3) As previously emphasized, the primary focus is on the amplitude when the excitation frequency exceeds 200 Hz. In the context of the four experimental conditions detailed in this study, the lowest vibration amplitude of the boring bar is achieved with a spring stiffness of 900 N/m. However, this finding deviates from the earlier simulation results. This discrepancy can be attributed to the fact that at very high stiffness levels, the inner core and the boring bar behave as a single entity, thereby rendering the damping boring bar no longer a two-degree-of-freedom system but a more complex dynamic system.

## 4. Conclusion

Vibration is an inherent phenomenon in machining processes. The DVA is recognized as an effective solution for vibration mitigation, owing to its simplicity in implementation and structure. To optimize the vibration reduction efficacy of the DVA, two critical aspects must be addressed: accurately determining the modal parameters of the cutting tool, and identifying the optimal spring stiffness, $k$. A combination of theoretical calculations and simulation methods is employed to ascertain these modal parameters, including the equivalent stiffness ($K$) and mass ($M$). Simulations conducted using Matlab reveal the relationship between spring stiffness and the vibration amplitude of the VCS. The results indicate an increase in the peak amplitude of the first-order natural frequency with higher stiffness. However, within the parameter $g$ range of 0.5 to 1.1, a decrease in amplitude is observed, suggesting that a larger stiffness is preferable for improved vibration reduction.

Experimental validation was performed through frequency sweep experiments on a damping boring bar using a vibration excitation platform. It was found that exceedingly high stiffness levels cause the inner core and the boring bar to function as a single unit, thereby altering the system's dynamics from a two-degree-of-freedom to a more complex state. Consequently, excessively high stiffness does not yield optimal vibration reduction. Thus, it is imperative to select a stiffness level that is appropriate for the specific machining model to achieve the best vibration reduction outcome.

## Acknowledgement

This work is supported by the Natural Science Foundation of the Jiangsu Higher Education Institutions of China (Grant No. 20KJB460018), the Research Fund for Doctoral Degree Teachers of Jiangsu Normal University, China (Grant No. 20XSRS014), the National Natural Science Foundation of China (Grant No. 12302013 Study on nonlinear dynamic characteristics and vibration suppression mechanism of an air-supported boring bar), the Practice Innovation Training Program for College Students, China (Grant No. 202110320087Y).

## References

[1] Quintana, G., Ciurana, J. (2011). Chatter in machining processes: A review, *International Journal of Machine Tools and Manufacture*, Vol. 51, No. 5, 363-376, doi: 10.1016/j.ijmachtools.2011.01.001.

[2] Okokpujie, I.P., Sinebe, J.E. (2023). An overview of the study of ANN-GA, ANN-PSO, ANFIS-GA, ANFIS-PSO and ANFIS-FCM predictions analysis on tool wear during machining process, *Journal Européen des Systèmes Automatisés,* Vol. 56, No. 2, 269-280, doi: 10.18280/jesa.560212.

[3] Siddhpura, M., Paurobally, R. (2012). A review of chatter vibration research in turning, *International Journal of Machine Tools and Manufacture,* Vol. 61, 27-47, doi: 10.1016/j.ijmachtools.2012.05.007.

[4] Antonucci, A., Coltrinari, G., Lippiello, D. (2023). Effectiveness of antivibration gloves when used with a light electric hammer, Differences among different methods of measurements, *International Journal of Computational Methods and Experimental Measurements*, Vol. 11, No. 1, 27-34, doi: 10.18280/ijcmem.110104.

[5] Margabandu, V., Radhakrishnan, R. (2021). Multi objective study on machining characteristics of AISI H-11 tool steel prepared by different processing techniques, *Journal Européen des Systèmes Automatisés,* Vol. 54, No. 2, 243-251, doi: 10.18280/jesa.540206.

[6] Okokpujie, I.P., Tartibu, L.K. (2022). Comparative study of the effect of dry, mineral oil, and TiO2 nano-lubricant on tool wear during face-milling machining of Ti-6al-4v-Eli using carbide tool insert, *Mathematical Modelling of Engineering Problems,* Vol. 9, No. 2, 468-476, doi: 10.18280/mmep.090224.

[7] Gao, H.N., Shen, H.D., Yu, L., Wang, Y.L., Yang, Y., Yan, S.C., Hu, Y.J. (2021). Frictional wear detection of hard alloy tool material during high-speed cutting, *International Journal of Heat and Technology,* Vol. 39, No. 6, 1845-1852, doi: 10.18280/ijht.390619.

[8] Jasiewicz, M., Miądlicki, K. (2020). An integrated CNC system for chatter suppression in turning, *Advances in Production Engineering & Management*, Vol. 15, No. 3, 318-330, doi: 10.14743/apem2020.3.368.

[9] Li, L., Sun, B., He, M. (2019). Analysis of radial stiffness of rubber bush used in dynamic vibration absorber, *Journal of Southeast University (English Edition)*, Vol. 35, No. 3, 281-287.

[10] Vukelic, D., Prica, M., Ivanov, V., Jovicic, G., Budak, I., Luzanin, O. (2022). Optimization of surface roughness based on turning parameters and insert geometry, *International Journal of Simulation Modelling*, Vol. 21, No. 3, 417-428, doi: 10.2507/IJSIMM21-3-607.

[11] Rubio, L., Loya, J.A., Miguélez, M.H., Fernández-Sáez, J. (2013). Optimization of passive vibration absorbers to reduce chatter in boring, *Mechanical Systems and Signal Processing*, Vol. 41, No. 1-2, 691-704, doi: 10.1016/j.ymssp.2013.07.019.

[12] Kang, W.T., Derani, M.N., Ratnam, M.M. (2020). Effect of vibration on surface roughness in finish turning: Simulation study, *International Journal of Simulation Modelling*, Vol. 19, No. 4, 595-606, doi: 10.2507/IJSIMM19-4-531.
[13] Vukelic, D., Simunovic, K., Kanovic, Z., Saric, T., Doroslovacki, K., Prica, M., Simunovic, G. (2022). Modelling surface roughness in finish turning as a function of cutting tool geometry using the response surface method, Gaussian process regression and decision tree regression, *Advances in Production Engineering & Management*, Vol. 17, No. 3, 367-380, doi: 10.14743/apem2022.3.442.
[14] Ormondroyd, J., Den Hartog, J.P. (1928). The theory of the dynamic vibration absorber, *ASME Journal of Applied Mechanics,* Vol. 50, No. 7, 9-22.
[15] Miguélez, M.H., Rubio, L., Loya, J.A., Fernández-Sáez, J. (2010). Improvement of chatter stability in boring operations with passive vibration absorbers, *International Journal of Mechanical Sciences*, Vol. 52, No. 10, 1376-1384, doi: 10.1016/j.ijmecsci.2010.07.003.
[16] Li, L., Sun, B. (2016). Optimal parameters selection and engineering implementation of dynamic vibration absorber attached to boring bar, In: *Proceedings of the INTER-NOISE and NOISE-CON Congress and Conference,* Hamburg, Germany, 563-570.
[17] Li, L., Sun, B., Hua, H. (2019). Nonlinear system modeling and damping implementation of a boring bar, *International Journal of Advanced Manufacturing Technology*, Vol. 104, 921-930, doi: 10.1007/s00170-019-03907-8.
[18] Li, L., Sun, B., Hua, H. (2019). Analysis of the vibration characteristics of a boring bar with a variable stiffness dynamic vibration absorber, *Shock and Vibration*, Vol. 2019, Article ID 5284194, doi: 10.1155/2019/5284194.
[19] Brock, J.E. (1946). A note on the damped vibration absorber, *ASME Journal of Applied Mechanics,* Vol. 13, No. 4, Article No. A-284, doi: 10.1115/1.4009588.
[20] Åkesson, H., Smirnova, T., Håkansson, L. (2009). Analysis of dynamic properties of boring bars concerning different clamping conditions, *Mechanical Systems and Signal Processing*, Vol. 23, No. 8, 2629-2647, doi: 10.1016/j.ymssp.2009.05.012.
[21] Andrén, L., Håkansson, L., Brandt, A., Claesson, I. (2004). Identification of dynamic properties of boring bar vibrations in a continuous boring operation, *Mechanical Systems and Signal Processing*, Vol. 18, No. 4, 869-901, doi: 10.1016/S0888-3270(03)00093-1.
[22] Zhang, G.M., Kapoor, S.G. (1987). Dynamic modeling and analysis of the boring machining system, *ASME Journal of Engineering for Industry,* Vol. 109, No. 3, 219-226, doi: 10.1115/1.3187122.
[23] Parker, E.W. (1970). Dynamic stability of a cantilever boring bar with machined flats under regenerative cutting conditions, *Journal of Mechanical Engineering Science*, Vol. 12, No. 2, 104-115, doi: 10.1243/JMES_JOUR_1970_012_018_02.
[24] Tewani, S.G., Rouch, K.E., Walcott, B.L. (1995). A study of cutting process stability of a boring bar with active dynamic absorber, *International Journal of Machine Tools and Manufacture*, Vol. 35, No. 1, 91-108, doi: 10.1016/0890-6955(95)80009-3.
[25] Seto, K., Yamada, K. (1980). An investigation on boring bars equipped with a dynamic absorber, In: *Proceeding of the 4th International Conference on Production Engineering*, Tokyo, Japan, 422-427.